observed in the brain and cognitive deficiency present in these patients is variable. Recently much attention has been given to the genotype–phenotype correlations based on the breakpoints distal to *PAFAH1B1* in 17p13.3 [Bi et al., 2009].

Here, we report on the case of a girl with mild developmental delay but normal brain structure on MRI, with a terminal deletion of 17p13.3 that involved *YWHAE*, but not *PAFAH1B1*, as demonstrated by FISH and gene expression studies. These results imply that YWHAE is associated with a complex mechanism of neuronal development.

CLINICAL REPORT

The 5-year-old girl was born at 40 weeks of gestation by cesarean due to fetal distress, to healthy, non-consanguineous parents. The father and mother were 34 and 33 years old, respectively, and previously had a healthy son. There was no family history of epilepsy and intellectual disability. The girl's birth weight was 2,156 g, length 46 cm, and occipito-frontal circumference (OFC) 33.6 cm, respectively. Her Apgar scores were 6/8. She was hospitalized for severe congenital anemia, caused by feto-maternal transfusion syndrome, and persistent pulmonary hypertension of the newborn.

Developmental milestones were mildly delayed; head control was achieved by 4 months, sitting by 8 months, walking by 18 months, single word by first year, and two-word phrase by 2 years. At 3 years, a ligation procedure for the patent ductus arteriosus was performed. The developmental quotient (DQ), using the Kyoto Scale for Psychological Development, was 70 at the age of 4 years and 9 months. At this age, she presented febrile convulsion lasting 1 min. Biochemical analysis revealed normal levels of insulin-like growth factor-1 (IGF-1), basal growth hormone (GH), thyroid function, cortisol, adrenocorticotropic hormone (ACTH), and prolactin. GH levels in response to stimulation tests were normal for her age. However, growth hormone therapy was started from the age of 4 years as growth retardation had been noted from infancy; this was effective to achieve catch-up growth. Standard karyotyping was normal.

On examination at the age of 5 years, her height was 97.5 cm (−2.4 SD), weight 14.1 kg (−1.5 SD), and OFC 51.4 cm (+0.6 SD). Her facial appearance was distinctive characterized by macrocephaly, a high forehead, hypertelorism, and thin upper lip vermilion (Fig. 1). Brain MRI at 3 T showed almost normal appearances without any structural abnormality but faint patchy high-intensity areas in the frontal subcortical white matter on T2-weighted and fluid attenuated inversion recovery (FLAIR) images (Fig. 2).

MATERIALS AND METHODS

Written informed consent was obtained from the parents of the patient in accordance with the Kanagawa Children's Medical Center Review Board and Ethics Committee.

Molecular Cytogenetic and Array CGH Investigations

An initial FISH analysis for patients with DD/ID and/or multiple congenital anomalies (MCA) was carried out with subtelomeric probes (Vysis, Downers Grove, IL) according to the standard protocol. A probe specific for Miller–Dieker syndrome (LIS1; Vysis) was also used.

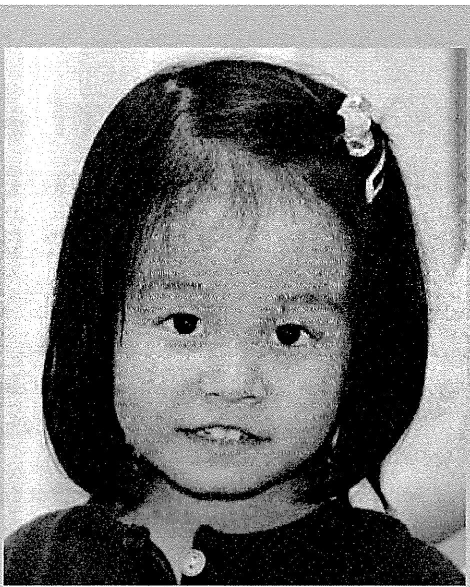

FIG. 1. Patient at the age of 5 years, showing the high forehead, broad nasal root, and thin upper lip vermilion.

Further FISH analysis for determining the breakpoint on 17p13.3 was carried out using bacterial artificial chromosome (BAC) clones that were selected from the May 2004 (NCBI35/hg17) Assembly of the UCSC Genome Browser (http://genome.ucsc.edu/) for Human. A centromere probe for chromosome 17 was used to confirm chromosome 17.

All DNAs were labeled by nick translation, according to the manufacturer's instructions (Vysis). Hybridization, post-hybridization washing, and counterstaining were performed according to standard procedures. Slides were analyzed using a completely motorized epifluorescene microscope (Leica DMRXA2) equipped with CCD camera. Both the camera and microscope were controlled with Leica CW4000 M-FISH software (Leica Microsystems Imaging Solutions, Cambridge, UK) [Yamamoto et al., 2009].

Array-CGH was performed using the Agilent SurePrint G3 Human CGH Microarray Kit 8×60K (Agilent Technologies, Inc., Santa Clara, CA) according the manufacturer's instructions. The total genomic DNA of the patient was prepared using the standard techniques. The results were analyzed using Agilent Genomic Workbench software. Only experiments having a DLR spread value <0.30 were taken into consideration.

Real-Time PCR

YWHAE is highly conserved and is ubiquitously expressed, but is expressed at highest levels in the brain [Toyo-oka et al., 2003]. To reduce the effects of SNP of *YWHAE* or other genes studied in each subject, we used lymphoblastoid cell lines [Ikeda et al., 2008].

Total RNA from lymphoblastoid cell lines were isolated with the use of a QIAamp RNA Blood Mini Kit (QIAGEN, Valencia, CA).

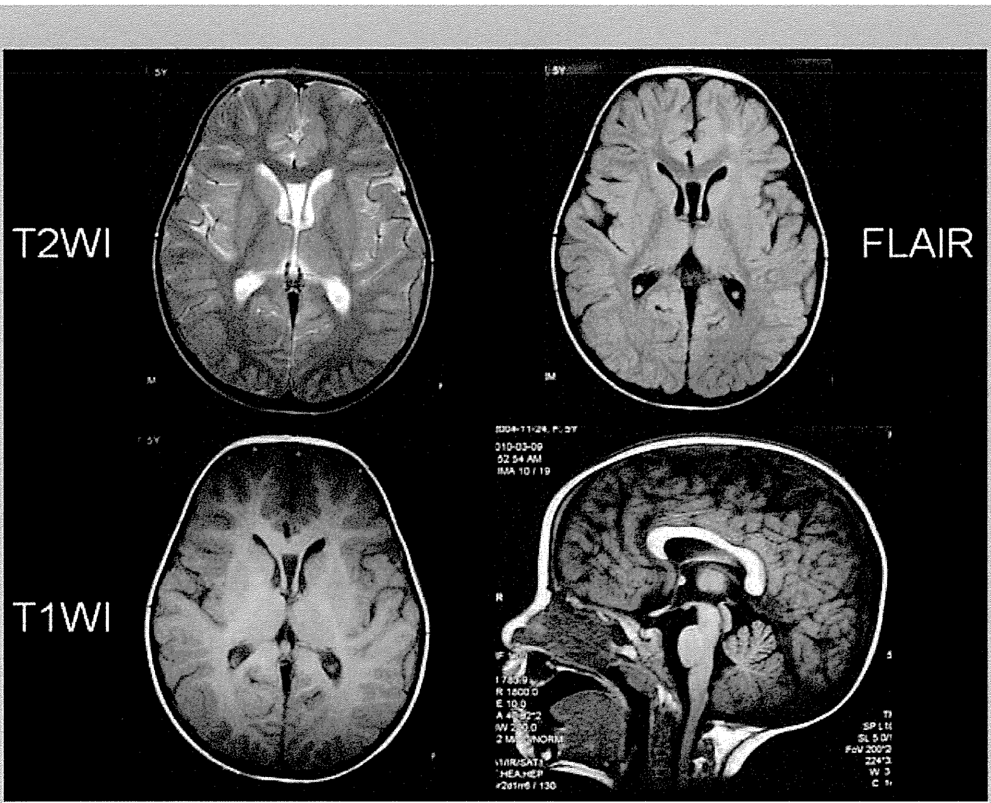

FIG. 2. Brain MRI at the age of 5 years. T1-, T2-weighted, and FLAIR images at 3-Tesla show no clinically significant abnormality but faint patchy high-intensity areas in the frontal subcortical white matter on T2-weighted and FLAIR images.

One microgram of total RNA was used for first-strand cDNA synthesis, using a Transcriptor High Fidelity cDNA synthesis kit (Roche Diagnostics, Rotkreuz, Switzerland). Real-time reverse transcription PCR was performed in a LightCycler 480 (Roche Diagnostics) using SYBR green, under the following cycling conditions: 10 min at 95°C, 45 cycles at 95°C for 30 sec, 60°C for 30 sec, and 72°C for 15 sec. The forward and reverse primer sequences used for *YWHAE* were 5′-GGATACGCTGAGTGAAGAAAGC-3′ and 5′-TATTCTGCTCTTCACCGTCACC-3′; for *PAFAH1B1*, primers were 5′-ATGGTCTCTGCTTCAGAGGATG-3′ and 5′-GTCATATCTGCAGAACAGGAAGC-3′. Beta-actin was chosen as the reference gene. Statistical analysis was performed using the delta–delta CT method. Lymphoblastoid cell lines from the patient's parents, as well as from a patient with Miller–Dieker syndrome caused by submicroscopic translocation of 17p13.3, including *PAFAH1B1* [Masuno et al., 1995], and from normal females were used for the control materials.

RESULTS

Molecular Cytogenetic and Array CGH Investigations

The complete subtelomere probe set analysis detected a 17pter deletion in the patient. However, the LIS1 probe signal was retained in the derivative chromosome. To characterize the size of the deletion, we further applied FISH analysis using the BAC clones that mapped to the region (Supplementary eFig. 1—See Supporting Information online). This revealed that the breakpoint was just on the telomeric site of the *PAFAH1B1* gene, about 2.44 Mb from 17pter (Fig. 3). The deleted region included *YWHAE* and *CRK*. Exclusion of mosaicism of the 17pter deletion was confirmed by observation on more than 100 cells.

Subsequent array CGH analysis revealed a 17p13.3 terminal microdeletion of approximately 2.3 Mb in size (chr17: −2,371, 138), which is consistent with the FISH results. No other genomic imbalances were identified on the array analysis. FISH analysis with relevant BAC clones indicated that the translocation was absent in both parents, and therefore had occurred de novo.

Real-Time PCR of YWHAE and PAFAH1B1 mRNA

We compared the expression level of *YWHAE* mRNA between the patient, her parents, a Miller–Dieker syndrome patient, and normal female controls by quantitative real-time PCR (Fig. 4). The relative expression levels were standardized to those of the patient with Miller–Dieker syndrome, which entails haploinsufficiency for both *YWHAE* and *PAFAH1B1*. We found that the *YWHAE* gene expression level in the patient was equal to that in the Miller–Dieker

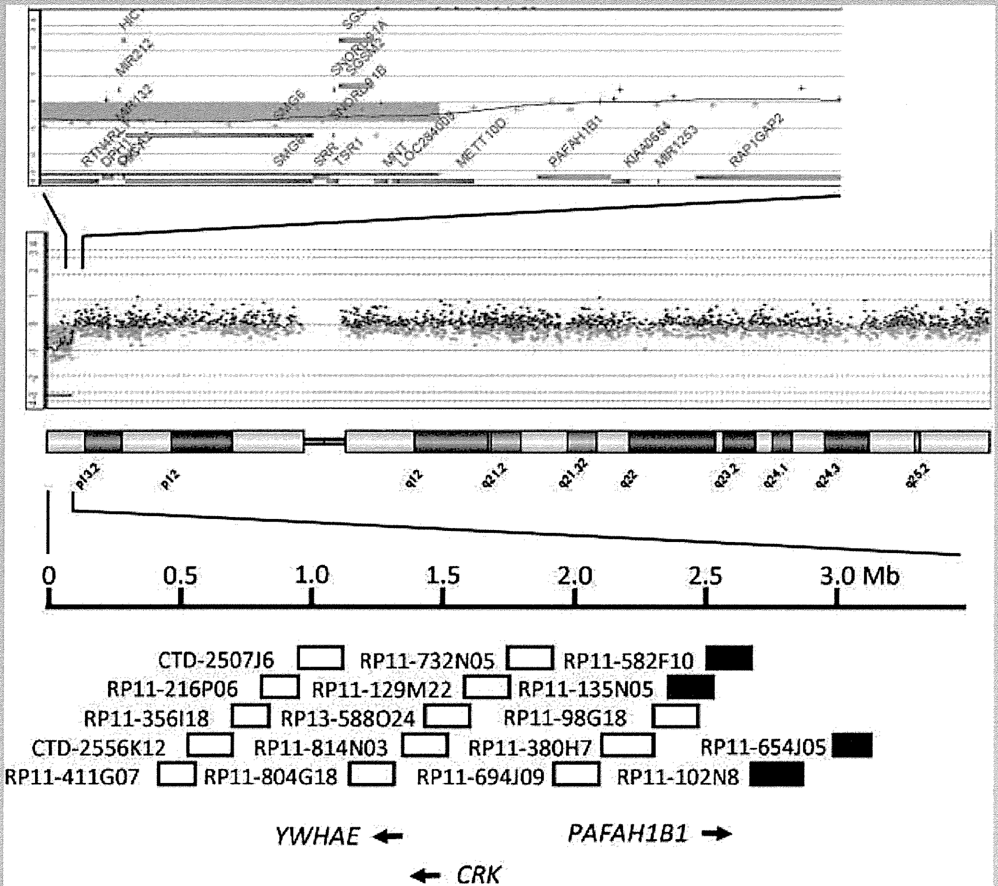

FIG. 3. Schematic representation of 17p13.3 region and bacterial artificial chromosome (BAC) clones used for refinement of the breakpoint derived from the results from array analysis. The map and position of the BAC clones are based on the information from the USCS Genome Browser (Assembly 2004, NCBI35/hg17) and Human 32K BAC Re-Array from Children's Hospital Oakland Research Institute (CHORI) BACPAC Resource. Signal retention was detected at RP11-135N5, but not at RP11-98F18, demonstrating that the breakpoint was just distal from *PAFAH1B1*. The deleted clones are indicated by open boxes, and non-deleted clones by full boxes.

syndrome patient, but was half that of her parents and normal controls. However, the expression level of *PAFAH1B1* in the patient was equal to that of the controls, but was twofold that of Miller–Dieker syndrome patient. These results were consistent with the molecular cytogenetic results.

DISCUSSION

Microdeletion of 17p13.3 involving *YWHAE*, but distal to *PAFAH1B1*, is a newly recognized syndrome associated with variable disorders of cortical development and facial dysmorphism. Here, we describe identification of a terminal microdeletion of 17p13.3 involving the *YWHAE* gene and *CRK* gene but not *PAFAH1B1*, in a girl, who had experienced mild developmental delay, short stature, and had a distinctive facial appearance, but who demonstrated normal cortical development on MRI. Expression studies of *YWHAE* and *PAFAH1B1* correlated with FISH results. This is the first report of evidence of dosage effects of the *YWHAE* gene in a patient with 17p13.3 microdeletion. *YWHAE* haploinsufficiency results in brain malformation, including cortical defects and corpus callosum hypoplasia, in both mice and humans [Toyooka et al., 2003; Mignon-Ravix et al., 2010]. However, the present case demonstrated normal brain structure on MRI. The structural brain abnormalities in patients with deletion of *YWHAE*, but not *PAFAH1B1*, have been shown to be variable; this variation included normal MRI findings [Nagamani et al., 2009; Bruno et al., 2010; Mignon-Ravix et al., 2010; Schiff et al., 2010; Shimojima et al., 2010; Tenney et al., 2011]. To our knowledge, two other cases with *YWHAE* deletion, but without obvious abnormalities on MRI, have been reported (Case DR00-063a1 in Cardoso et al. [2003], Patient 3 in Nagamani et al. [2009]). The structural variation of the brain and severity of intellectual disability or development

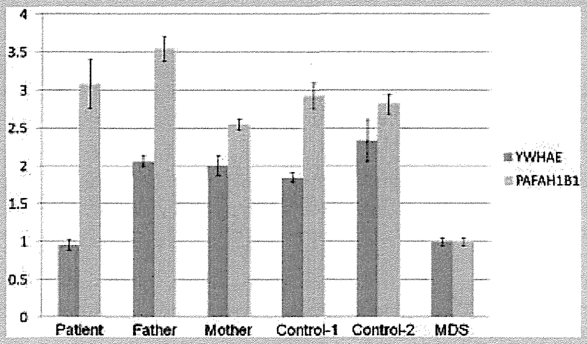

FIG. 4. Expression of *YWHAE* and *PAFAH1B1*. Quantitative measurements were standardized to the expression level in the patients with Miller–Dieker syndrome. These results were consistent with the genome copy number of each subject as indicated by FISH analysis.

represented no strict correlation in the cases with deletion of *YWHAE* but not *PAFAH1B1* (Fig. 5). These results indicated that the YWHAE plays a crucial role in neuronal development in humans, but does not result in structural abnormalities of the brain in a haploinsufficiency state. This is in contrast to *PAFAH1B1*; haploinsufficiency of this gene alone contributes to lissencephaly.

YWHAE has been shown to function within a complex with several other factors, such as PAFAH1B1 and NUDEL. Recently, using the global gene expression and pathway analysis in targeted gene mutations of *Lis1*, *Dcx*, *Ywhae*, and *Ndel1*, Pramparo et al. [2011] demonstrated that cell cycle and synaptogenesis genes are similarly expressed and are co-regulated in the developing brains of normal and mutant mouse in a time-dependent manner. Thus, reduced expression levels of *YWHAE* may still be able to mediate normal brain structure, as detected by MRI in humans [Bruno et al., 2010]. Further analysis of correlation between clinical phenotype and expression levels of related genes in brain development are required for elucidating the mechanism of neurodevelopmental disorders associated with mutations involving *YWHAE*.

The present patient we described here showed prenatal onset of growth retardation, in the absence of growth hormone deficiency; however, growth hormone therapy was effective in mediating catch-up growth from the age of 4 years. Prenatal onset of severe growth retardation is common to patients with deletions of the subtelomeric region of 17p13.3 involving *YWHAE*. However, in those cases with small, limited deletions involving *YWHAE*, growth retardation is not so as severe, as seen in Patient 1 reported by Nagamani et al. [2009] and the patient described by Mignon-Ravix et al. [2010]. Therefore, evaluation of hormones associated with growth in patients with a 17p13.3 microdeletion will also provide further insights into the genotype–phenotype correlations attributed to genes involved in these disorders.

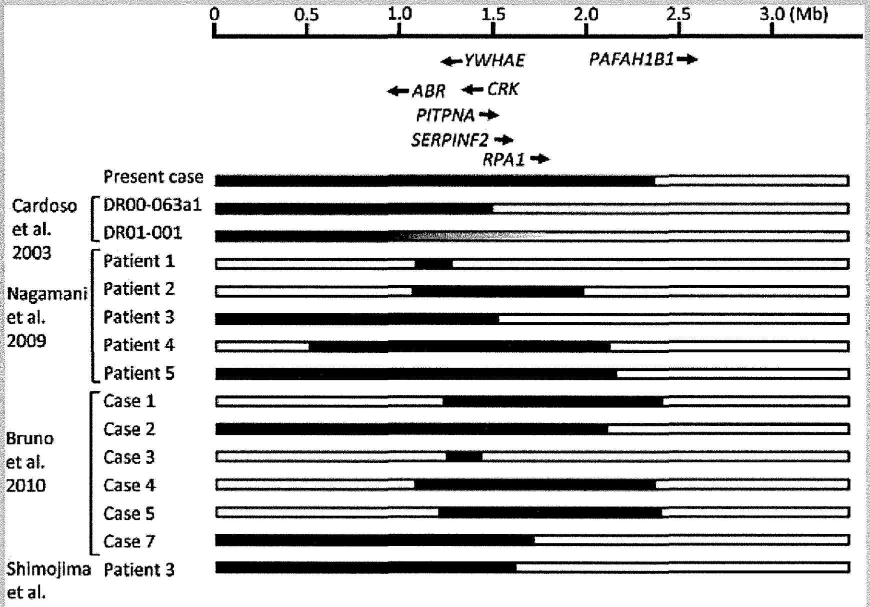

FIG. 5. Schematic representation of the microdeletion 17p13.3 including *YWHAE*, but not *PAFAH1B1*. The dark horizontal bars indicate the range of the deletion of reported patients.

ACKNOWLEDGMENTS

We thank the patient and her family for making this study possible. We are also grateful to Dr. Shuki Mizutani (Tokyo Medical and Dental University) and Dr. Hiroyuki Ida (Tokyo Jikei University) for their valuable comments. This research was supported in part by a Grant-in-aid from the Ministry of Health, Labour and Welfare, Japan.

REFERENCES

Bi W, Sapir T, Shchelochkov OA, Zhang F, Withers MA, Hunter JV, Levy T, Shinder V, Peiffer DA, Gunderson KL, Nezarati MM, Shotts VA, Amato SS, Savage SK, Harris DJ, Day-Salvatore D-L, Horner M, Lu X-Y, Sahoo T, Yanagawa Y, Beaudet AL, Cheung SW, Martinez S, Lupski JR, Reiner O. 2009. Increased LIS1 expression affects human and mouse brain development. Nat Genet 41:168–177.

Bruno DL, Anderlid BM, Lindstrand A, van Ravenswaaij-Arts C, Ganesamoorthy D, Lundin J, Martin CL, Douglas J, Nowak C, Adam MP, Kooy RF, Van der Aa N, Reyniers E, Vandeweyer G, Stolte-Dijkstra I, Dijkhuizen T, Yeung A, Delatycki M, Borgström B, Thelin L, Cardoso C, van Bon B, Pfundt R, de Vries BB, Wallin A, Amor DJ, James PA, Slater HR, Schoumans J. 2010. Further molecular and clinical delineation of co-locating 17p13.3 microdeletions and microduplications that show distinctive phenotypes. J Med Genet 47:299–311.

Cardoso C, Leventer RJ, Ward HL, Toyo-Oka K, Chung J, Gross A, Martin CL, Alanson J, Pills DT, Olney AH, Mutchinick OM, Hirotsune S, Wynshaw-Boris A, Dobyns WB, Ledbetter DH. 2003. Refinement of 400-kb critical region allows genotypic differentiation between isolated lissencepahly, Miller-Dieker syndrome, and other phenotypes secondary to deletions of 17p13.3. Am J Hum Genet 72:918–930.

Dobyns WB, Reiner O, Carrozzo R, Ledbetter DH. 1993. Lissencephaly. A human brain malformation associated with deletion of the LIS1 gene located at chromosome 17p13. JAMA 270:2838–2842(Review).

Ikeda M, Hikita T, Taya S, Uraguchi-Asaki J, Toyo-oka K, Wynshaw-Boris A, Ujike H, Inada T, Takao K, Miyakawa T, Ozaki N, Kaibuchi K, Iwata N. 2008. Identification of YWHAE, a gene encoding 14-3-3 epsilon, as a possible susceptibility gene for schizophrenia. Hum Mol Genet 17: 3212–3222.

Masuno M, Imaizumi K, Nakamura M, Matsui K, Goto A, Kuroki Y. 1995. Miller-Dieker syndrome due to maternal cryptic translocation t(10;17)-(q26.3;p13.3). Am J Med Genet 59:441–443.

Mignon-Ravix C, Cacciagli P, El-Waly B, Moncla A, Milh M, Girard N, Chabrol B, Philip N, Villard L. 2010. Deletion of YWHAE in a patient with periventricular heterotopias and pronounced corpus callosum hypoplasia. J Med Genet 47:132–136.

Nagamani SC, Zhang F, Shchelochkov OA, Bi W, Ou Z, Scaglia F, Probst FJ, Shinawi M, Eng C, Hunter JV, Sparagana S, Lagoe E, Fong CT, Pearson M, Doco-Fenzy M, Landais E, Mozelle M, Chinault AC, Patel A, Bacino CA, Sahoo T, Kang SH, Cheung SW, Lupski JR, Stankiewicz P. 2009. Microdeletions including YWHAE in the Miller-Dieker syndrome region on chromosome 17p13.3 result in facial dysmorphisms, growth restriction, and cognitive impairment. J Med Genet 46:825–833.

Pramparo T, Libiger O, Jain S, Li H, Youn YH, Hirotsune S, Schork NJ, Wynshaw-Boris A. 2011. Global developmental gene expression and pathway analysis of normal brain development and mouse models of human neuronal migration defects. PLoS Genet 7:e1001331.

Schiff M, Delahaye A, Andrieux J, Sanlaville D, Vincent-Delorme C, Aboura A, Benzacken B, Bouquillon S, Elmaleh-Berges M, Labalme A, Passemard S, Perrin L, Manouvrier-Hanu S, Edery P, Verloes A, Drunat S. 2010. Further delineation of the 17p13.3 microdeletion involving YWHAE but distal to PAFAH1B1: Four additional patients. Eur J Med Genet 53:303–308.

Shimojima K, Sugiura C, Takahashi H, Ikegami M, Takahashi Y, Ohno K, Matsuo M, Saito K, Yamamoto T. 2010. Genomic copy number variations at 17p13.3 and epileptogenesis. Epilepsy Res 89:303–309.

Tenney JR, Hopkin RJ, Schapiro MB. 2011. Deletion of 14-3-3{varepsilon} and CRK: A clinical syndrome with macrocephaly. Developmental delay, and generalized epilepsy. J Child Neurol 26:223–227.

Toyo-oka K, Shionoya A, Gambello MJ, Cardoso C, Leventer R, Ward HL, Ayala R, Tsai LH, Dobyns W, Ledbetter D, Hirotsune S, Wynshaw-Boris A. 2003. 14-3-3 Epsilon is important for neuronal migration by binding to NUDEL: A molecular explanation for Miller-Dieker syndrome. Nat Genet 34:274–285.

Yamamoto K, Yoshihashi H, Furuya N, Adachi M, Ito S, Tanaka Y, Masuno M, Chiyo H, Kurosawa K. 2009. Further delineation of 9q22 deletion syndrome associated with basal cell nevus (Gorlin) syndrome: Report of two cases and review of the literature. Congenit Anom (Kyoto) 49:8–14.

Pediatr Radiol (2012) 42:380–382
DOI 10.1007/s00247-011-2156-6

CASE REPORT

A case of Sjögren-Larsson syndrome with minimal MR imaging findings facilitated by proton spectroscopy

Yasuhiko Tachibana · Noriko Aida · Keisuke Enomoto ·
Mizue Iai · Kenji Kurosawa

Received: 7 March 2011 / Revised: 2 May 2011 / Accepted: 6 May 2011 / Published online: 29 June 2011
© Springer-Verlag 2011

Abstract We present a 5-year-old girl who was ultimately diagnosed with Sjögren-Larsson syndrome (SLS). Although her MRI findings were minimal compared to previously published cases, prominent and characteristic abnormal lipid peaks on single-voxel proton MR spectroscopy (^{1}H-MRS) facilitated the diagnosis. This case emphasizes the importance and usefulness of ^{1}H-MRS in diagnosing SLS.

Keywords Sjögren-Larsson syndrome · MR spectroscopy · Lipids · Molecular study

Introduction

Sjögren-Larsson syndrome (SLS) is a rare autosomal-recessive neurocutaneous disorder characterized by a clinical triad of congenital ichthyosis, spastic diplegia or tetraplegia and mental retardation. The symptoms may be apparent at birth, and the syndrome usually develops in the first years of life [1]. The severity of the symptoms is variable and a few cases have very mild symptoms [2]; however, some hyperkeratosis seems inevitable. SLS is caused by deficiency of the microsomal enzyme fatty aldehyde dehydrogenase (FALDH) due to mutations in the *ALDH3A2* gene [3]. This results in accumulation of fatty alcohols, modification of macromolecules by fatty aldehydes and the presence of high concentrations of biologically active lipids, which have been postulated to be the pathophysiological mechanism of symptoms in SLS [1]. Previous studies regarding proton MR spectroscopy (^{1}H-MRS) of the brain in SLS patients have revealed abnormal lipid peaks at 1.3 ppm and/or 0.9 ppm [1], in addition to the characteristic MRI findings including a zone of abnormal high signal intensity in the periventricular white matter on T2-weighted images and delayed myelination development [1].

We present a girl with SLS whose brain MRI findings were minimal and nonspecific but who had prominent lipid peaks on ^{1}H-MRS. The suspicion of SLS was facilitated by this finding on ^{1}H-MRS in addition to her clinical symptoms. A distinct diagnosis based on a molecular analysis of her *ALDH3A2* gene was made.

Case report

The girl, born at 39 weeks' gestation to unrelated healthy parents, was 5 years old when she underwent MRI/^{1}H-MRS examination to evaluate unexplained lower limb spasticity. Her skin was normal in her first months of life, but hyperkeratosis on her trunk and limbs appeared in her first year of life, and developed into acanthosis and ichthyosis in the next year. However, SLS was not considered at the time. Her motor development was mildly delayed, with her achieving head control at 4 months, rolling over at 6 months, crawling at 12 months and walking without support at 21 months of age. She had a spastic gait with

Y. Tachibana (✉) · N. Aida
Department of Radiology, Kanagawa Children's Medical Center,
2-138-4 Mutsukawa, Minami-ku,
Yokohama, 232-8555, Japan
e-mail: yaz.tachibana@radio.email.ne.jp

K. Enomoto · K. Kurosawa
Division of Medical Genetics,
Kanagawa Children's Medical Center,
Yokohama, Japan

M. Iai
Department of Neurology, Kanagawa Children's Medical Center,
Yokohama, Japan

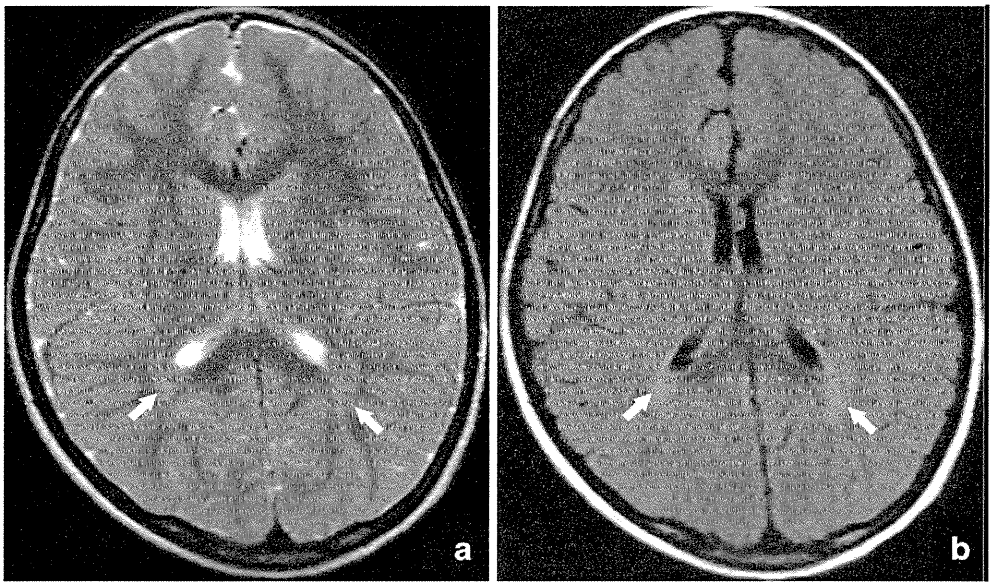

Fig. 1 MRI findings. **a** T2-weighted image (TR/TE=3,880/119 msec) and (**b**) T2-weighted fluid-attenuated inversion recovery image (TR/TE/TI=9,000/116/2,406 msec). The minimal high-intensity lesions in the deep white matter around the trigones of the bilateral lateral ventricles are scarcely distinguishable from a normal nonmyelinated lesion considering her age (*arrows*). TR = repetition time, TE = echo time, TI = inversion time

brisk deep tendon reflexes in her bilateral lower limbs, and developed worsening spasticity during her first 2 years. She had no deficiencies in intellectual development.

MR examinations were performed on a 1.5-T MRI system (Siemens MAGNETOM Avanto, Siemens Medical Solutions, Erlangen, Germany), by using a 12-channel head coil. ^{1}H-MRS was added to the MRI brain imaging sequences (i.e. transverse and sagittal T1-weighted spin-echo imaging, transverse and coronal T2-weighted fast spin-echo imaging, transverse diffusion-weighted imaging, and T2-weighted fluid-attenuated inversion recovery imaging (FLAIR), as is routinely done at our clinics when patients have neurological findings as in this case. ^{1}H-MRS was acquired by the single-voxel point resolved spectroscopy (PRESS) sequence. Repetition time (TR), echo time (TE) and the number of excitations (NEX) was set to 5,000 msec, 30 msec and 6, respectively. The volume of interest was set to the left centrum-semiovale (where no MRI abnormality was seen), which measured 40 mm× 25 mm×25 mm (Fig. 2). To note, another ^{1}H-MRS with longer TE (TR/TE/NEX set to 5,000 msec/135 msec/15) was acquired at the same volume of interest in addition (Fig. 2), as described later.

T2-weighted images and FLAIR images demonstrated slight minimum high-intensity areas around the trigones of the bilateral lateral ventricles, which were hardly distinguishable from the terminal zone (Fig. 1). No other pathological finding was noted in the MRI examination. On the other hand, ^{1}H-MRS revealed a prominent and narrow abnormal peak at 1.3 ppm and a relatively small narrow peak at 0.9 ppm (Fig. 2). To exclude lactate from the peak at 1.3 ppm, the aforementioned additional ^{1}H-MRS with longer TE was acquired at the same volume of interest. The peaks at 1.3 ppm and 0.9 ppm remained at this setting (Fig. 2), suggesting that they were derived from lipids, as the peak at 1.3 ppm would have been inverted if it

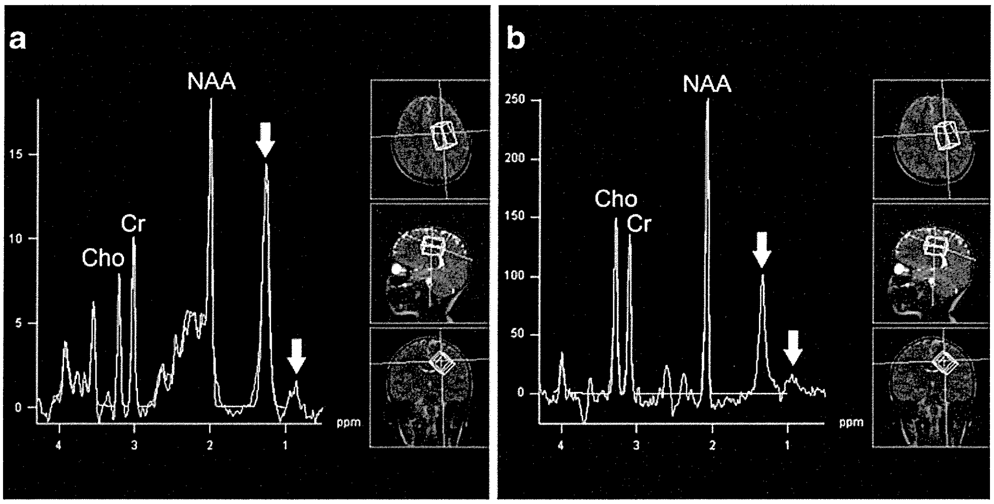

Fig. 2 MR spectroscopy. **a** Proton MR spectroscopy (^{1}H-MRS) (TR/TE/NEX=5,000 msec/30 msec/6) and (**b**) ^{1}H-MRS (TR/TE/NEX=5,000 msec/135 msec/15) both acquired at the same volume of interest at the left centrum-semiovale. Narrow abnormal resonance peaks at 1.3 ppm and 0.9 ppm are demonstrated in both (**a**) and (**b**) (*arrows*). NEX = number of excitations, *NAA* = N-acetyl aspartate, *Cr* = creatine, *Cho* = choline

were derived from lactate. A quantitative analysis based on LCModel was made and lipid peak at 1.3 ppm was confirmed. Other major molecules, including N-acetylaspartate, creatine, myo-inositol and choline, which were all within normal limits, were also comfirmed on LCModel. Based on the ^{1}H-MRS finding, in addition to the clinical symptoms, molecular analysis was conducted for suspicion of SLS.

Molecular analysis

Written informed consent was obtained from the girl's parents. Sequencing of all 11 exons and exon/intron junctions of the ALDH3A2 gene identified two mutations including c.1339A > G (p.K447E) in exon 9 and c.504_505insAG (p.Glu169ArgfsX8) in exon 4 in the heterozygote state, respectively. The first mutation is known as a disease-causing allele, resulting in reduced FALDH activity as low as 1% of normal [4]. The final diagnosis of SLS was made. Of note, the second mutation is a novel mutation of ALDH3A2 not previously described.

Discussion

This case emphasizes the importance and usefulness of ^{1}H-MRS in diagnosing SLS, since the genetic testing was difficult to be triggered from the mild clinical symptoms and nonspecific MRI findings alone. It is well known that SLS is characterized by unusual narrow and prominent resonance peaks at 1.3 ppm and 0.9 ppm in ^{1}H-MRS, which correspond to the resonance of lipids. This finding is observed in all SLS cases published to date without exception when ^{1}H-MRS was acquired from the deep cerebral white matter of the brain [1, 5]. The MRI findings of the present case may be milder than any of the others. Another case of SLS reported by Nakayama et al. [5] also demonstrates mild MRI findings despite the prominent lipid peak on ^{1}H-MRS, but we presume that the MRI findings of our case are even less notable, especially given that ^{1}H-MRS in our case was acquired from a region without any MRI abnormalities, compared to the previous case that acquired ^{1}H-MRS from an area with abnormal high intensity in T2-weighted imaging. Willemsen et al. [1] evaluated ^{1}H-MRS acquired from 18 SLS patients and reported elevated levels of creatine (+14%), choline (+18%) and myo-inositol (+54%) in addition to lipids, but the molecules other than lipids were not elevated in our case.

The prominent and narrow resonance at 1.3 ppm is where the protons of methylene groups ($-[CH_2]_n-$) resonate, while the resonance at 0.9 ppm is where the protons of methyl groups ($-[CH_2]_n-CH_3$) resonate. These peaks in SLS presumably represent lipids that accumulate because of the FALDH deficiency, which may be fatty alcohols, fatty aldehydes and their metabolites [1]. It may be important to note that the resonance at 1.3 ppm and 0.9 ppm is not specific to SLS. Previous studies reported unusual peaks at 1.3 ppm (and 0.9 ppm) in other pathological states, including peroxisomal diseases such as Zellweger syndrome [6] or rhizomelic chondrodysplasia punctata [7], and other diseases including cerebrotendinous xanthomatosis [8]. In those cases, the lipid peaks are less prominent and broader compared to SLS, and visualized only in a short echo time (e.g., 30 msec) in contrast to SLS, in which peaks are visualized in a longer echo time (135 msec in the presented case). However, we still may not make a diagnosis of SLS based solely on a finding of these abnormal peaks on ^{1}H-MRS because methylene groups and methyl groups are both quite common structures in organic matters, and many other diseases (including metabolic and storage disorders of higher fatty acids and/or higher hydrocarbon) or conditions of destroyed normal tissue may present similar abnormal peaks.

In patients without typical clinical symptoms or without prominent white matter abnormality on MRI, ^{1}H-MRS is a useful tool to facilitate an appropriate molecular survey to make a diagnosis of SLS.

References

1. Willemsen MA, Van Der Graaf M, Van Der Knaap MS et al (2004) MR imaging and proton MR spectroscopic studies in Sjogren-Larsson syndrome: characterization of the leukoencephalopathy. AJNR 25:649–657
2. Ganemo A, Jagell S, Vahlquist A (2009) Sjogren-larsson syndrome: a study of clinical symptoms and dermatological treatment in 34 Swedish patients. Acta Derm Venereol 89:68–73
3. Rizzo WB (2007) Sjogren-Larsson syndrome: molecular genetics and biochemical pathogenesis of fatty aldehyde dehydrogenase deficiency. Mol Genet Metab 90:1–9
4. Rizzo WB, Carney G, Lin Z (1999) The molecular basis of Sjogren-Larsson syndrome: mutation analysis of the fatty aldehyde dehydrogenase gene. Am J Hum Genet 65:1547–1560
5. Nakayama M, Tavora DG, Alvim TC et al (2006) MRI and 1H-MRS findings of three patients with Sjogren-Larsson syndrome. Arq Neuropsiquiatr 64:398–401
6. Bruhn H, Kruse B, Korenke GC et al (1992) Proton NMR spectroscopy of cerebral metabolic alterations in infantile peroxisomal disorders. J Comput Assist Tomogr 16:335–344
7. Viola A, Confort-Gouny S, Ranjeva JP et al (2002) MR imaging and MR spectroscopy in rhizomelic chondrodysplasia punctata. AJNR 23:480–483
8. Embirucu EK, Otaduy MC, Taneja AK et al (2010) MR spectroscopy detects lipid peaks in cerebrotendinous xanthomatosis. AJNR 31:1347–1349

Familial Cancer
DOI 10.1007/s10689-013-9623-1

ORIGINAL ARTICLE

Frameshift mutation in the *PTCH2* gene can cause nevoid basal cell carcinoma syndrome

Katsunori Fujii · Hirofumi Ohashi ·
Maiko Suzuki · Hiromi Hatsuse · Tadashi Shiohama ·
Hideki Uchikawa · Toshiyuki Miyashita

© Springer Science+Business Media Dordrecht 2013

Abstract Nevoid basal cell carcinoma syndrome (NBCCS) is an autosomal dominant disorder characterized by developmental defects and tumorigenesis. The gene responsible for NBCCS is *PTCH1*, encoding a receptor for the secreted protein, sonic hedgehog. Recently, a Chinese family with NBCCS carrying a missense mutation in *PTCH2*, a close homolog of *PTCH1*, was reported. However, the pathological significance of missense mutations should be discussed cautiously. Here, we report a 13-year-old girl diagnosed with NBCCS based on multiple keratocystic odontogenic tumors and rib anomalies carrying a frameshift mutation in the *PTCH2* gene (c.1172_1173delCT). Considering the deleterious nature of the frameshift mutation, our study further confirmed a causative role for the *PTCH2* mutation in NBCCS. The absence of typical phenotypes in this case such as palmar/plantar pits, macrocephaly, falx calcification, hypertelorism and coarse face, together with previously reported cases, suggested that individuals with NBCCS carrying a *PTCH2* mutation may have a milder phenotype than those with a *PTCH1* mutation.

Keywords Nevoid basal cell carcinoma syndrome · *PTCH1* · *PTCH2* · Frameshift mutation

K. Fujii · T. Shiohama · H. Uchikawa
Department of Pediatrics, Chiba University Graduate School of Medicine, Chiba 260-8670, Japan

H. Ohashi
Division of Medical Genetics, Saitama Children's Medical Center, Saitama 339-8551, Japan

M. Suzuki · H. Hatsuse · T. Miyashita (✉)
Department of Molecular Genetics, Kitasato University Graduate School of Medical Sciences, 1-15-1 Kitasato, Minami-ku, Sagamihara 252-0374, Japan
e-mail: tmiyashi@med.kitasato-u.ac.jp

Introduction

Nevoid basal cell carcinoma syndrome (NBCCS) (OMIM 109400), also known as Gorlin syndrome, is an autosomal dominant disorder characterized by developmental defects including bifid ribs, palmar or plantar pits, and tumorigenesis such as the development of basal cell carcinoma, medulloblastoma, or keratocystic odontogenic tumor (KCOT) (formerly known as odontogenic keratocysts) [1]. It is transmitted with complete penetrance and variable expressivity. The gene responsible for NBCCS is the human homologue of the *Drosophila patched* gene, *PTCH1* [2, 3]. The human *PTCH1* gene contains 23 coding exons spanning approximately 70 kb and encodes a protein of 1,447 amino-acid residues containing 12 transmembrane-spanning domains and two large extracellular loops [2]. The PTCH1 protein is the ligand-binding component of the sonic hedgehog (Shh) receptor complex. In the absence of Shh binding, PTCH1 is thought to hold smoothened (SMO), a 7-pass transmembrane protein, in an inactive state and thus inhibit signaling to downstream genes. Upon the binding of Shh, the inhibition of SMO is released and signaling is transduced leading to the activation of target genes by the Gli family of transcription factors [4]. Therefore, aberrant activation of the Shh signaling cascade due to the haploinsufficiency of *PTCH1* is believed to cause NBCCS.

In vertebrates, there exists a close homolog of *PTCH1* named *PTCH2*. The human *PTCH2* gene contains 22 coding exons spanning approximately 15 kb and encodes a protein of 1,203 amino-acid residues [5]. Recently, in six affected members of a Chinese Han family with NBCCS, Fan et al. identified a heterozygous germline missense mutation in the *PTCH2* gene [6]. Here we report a case with NBCCS carrying a frameshift mutation due to a 2-bp

Published online: 12 March 2013

deletion in *PTCH2*. To our knowledge, this is the first report of NBCCS caused by a frameshift mutation and the second report of a germline mutation in the *PTCH2* gene.

Clinical report

A 13-year-old Japanese girl was referred to our hospital with jaw cysts and a rib abnormality. She was born weighing 2,570 g, with a height of 48 cm and a head circumference of 32 cm. Her two siblings as well as her parents exhibited no similar features. No consanguineous marriage was noticed in her pedigree. At 10 years of age, she had multiple KCOTs (Fig. 1a) and underwent a surgical operation to remove them. At 12 years of age, she exhibited proteinuria, and was diagnosed as having chronic glomerular nephritis. Then, she was referred to our hospital for further investigation. At examination, she was 150.1 cm tall (mean) and weighed 57.8 kg (+1.8SD). Her head circumference was 54.6 cm (mean). She had normal intelligence without neurological deficit. She exhibited no structural abnormalities of face, oral cavity, or limbs. However, chest roentgenogram revealed a left bifid rib without any other bone abnormalities (Fig. 1b). She did not exhibit palmar or plantar pits, falx calcification, medulloblastomas, or basal cell carcinomas at that time. Since she exhibited KCOTs and a rib anomaly fulfilling the diagnostic criteria made by Kimonis et al. (two major criteria), we diagnosed her as having NBCCS.

Methods

DNA extraction and PCR-sequencing analysis

All experiments described below were approved by the ethics committee at Kitasato University. DNA was extracted from peripheral blood lymphocytes using a QIAamp DNA blood midi kit (QIAGEN). The complete coding region of the *PTCH1*, *PTCH2*, suppressor of fused (*SUFU*) and *SMO* genes, including all splice junctions, was amplified from constitutional DNA as described previously [7]. Primers used for amplifying *PTCH1*, *PTCH2* and *SUFU* exons were described previously [5, 7, 8]. Those used for amplifying *SMO* are listed in supporting information Table 1. Amplified products were gel-purified using a QIAEX II gel extraction kit (QIAGEN) and cycle sequenced with a BigDye Terminator v3.1 Cycle Sequencing Kit (Applied Biosystems) in both directions. The sequence was analyzed on a 3130 Genetic Analyzer (Applied Biosystems).

Comparison of clinical manifestations

Details of a nationwide survey of NBCCS performed in Japan have been described previously [9]. The survey covered 157 NBCCS patients whose clinical details were available. Major and minor criteria for NBCCS proposed by Kimonis et al. [10] were evaluated in these patients and compared with those observed in patients carrying a *PTCH2* mutation reported previously including the present case [6].

Results

No mutation in *PTCH1* or the related genes *SUFU* and *SMO* was detected in the peripheral blood from this patient. Although deletion of the entire *PTCH1* gene is a common event in point mutation-negative cases of NBCCS as we reported previously [11], no such deletion was observed using either a ligation-dependent probe amplification method or high-resolution array-based comparative genomic hybridization technology [11–13]. We then sequenced all exons of the *PTCH2* gene, since *PTCH2* is a close homolog of *PTCH1* and is also a suppressor component of the Shh pathway. As a result, a heterozygous 2-base-pair deletion, c.1172_1173delCT, was detected in exon 9 of *PTCH2* (Fig. 2). This mutation caused a frameshift and created a premature termination codon (PTC) at the site of the deletion resulting in a truncated form of the PTCH2 protein, p.S391X.

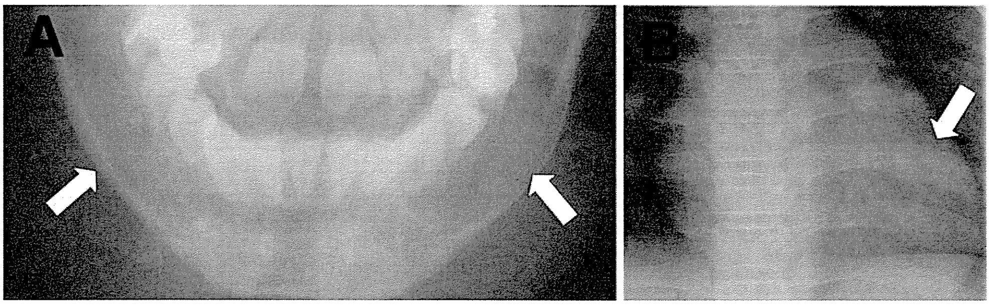

Fig. 1 Roentgenograms of the patient. **a** Pantomography shows bilateral keratocystic odontogenic tumors (*Arrows*). **b** Chest roentgenogram reveals a bifid anomaly of the left sixth rib (*Arrow*)

Table 1 Comparison of the characteristic phenotype of NBCCS in three groups

Patients	Number of patients	Mean age	Mean number of major criteria	Mean number of minor criteria
Nationwide survey	157	33.1	2.4*	1.3**
With *PTCH2* mutation	7	34.1	1.57	0.14

$^*P < 0.05$ (vs *PTCH2* mutation), ** $P < 0.01$ (vs *PTCH2* mutation)

In order to characterize the phenotype of individuals carrying a *PTCH2* mutation, we next evaluated the number of positive criteria for NBCCS proposed by Kimonis et al. [10] in two groups; first, NBCCS patients collected by a nationwide survey described previously [9], second, reported individuals carrying a *PTCH2* mutation including our case. In spite of the comparable mean ages in two groups (33.1 vs 34.1 years old), positivities of most of the criteria were lower in the *PTCH2* mutation-positive group than in the other, indicating that *PTCH2* mutations cause a milder phenotype than the classical NBCCS (Table 1). In fact, only 4 out of 7 individuals in the *PTCH2* mutation-positive group diagnosed as having NBCCS according to this diagnostic criteria.

Discussion

NBCCS is caused by a mutation in the gene *PTCH1*, with rare exceptions in which a *SUFU* mutation has been identified [8, 14, 15]. Recently, a heterozygous missense mutation in the *PTCH2* gene, c.2157G>A (p.R719Q), was identified in 6 affected members of a Chinese Han family with NBCCS [6]. Although the pathological significance of missense mutations should be discussed cautiously, this mutation was demonstrated to result in the inactivation of PTCH2's inhibitory activities at least in vitro. In this paper, we reported a second germline mutation of *PTCH2*, c.1172_1173delCT, found in a Japanese patient with NBCCS. This mutation created a PTC at the site of the deletion in the mutant allele, resulting in the truncation of the PTCH2 protein. However, since the PTC leads to the degradation of mRNA via a mechanism called nonsense-mediated mRNA decay [16], a haploinsufficiency of *PTCH2* is expected to play an important role in this case.

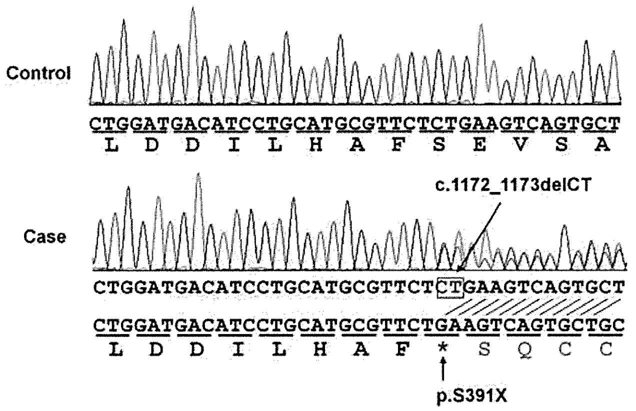

Fig. 2 Electropherograms of the *PTCH2* exon 9 sequence. DNA extracted from the peripheral blood of the patient (Case) as well as a healthy control (Control) was subjected to PCR direct sequencing. The predicted translation is indicated at the bottom of each electropherogram. PTC created by the deletion is indicated by an *asterisk*

Interestingly, this mutation is also present in the dbSNP database as rs56126236, submitted by the Center for Genome Medicine, Kyoto University Graduate School of Medicine, Japan. However, details such as frequency are unclear. Therefore, we analyzed 63 healthy Japanese individuals (126 alleles) on this mutation, but found none carrying this deletion. Thus, it is unlikely that this is a rare polymorphism at least in a Japanese population.

However, unfortunately, we were unable to get informed consents from family members and, therefore, could not add data regarding this issue. Nonetheless, considering the deleterious nature of the mutation, we believe that the mutation found in this patient is generated de novo.

Homozygous mutant mice, *Ptch2*$^{-/-}$, developed normally, were viable and fertile, and did not display any obvious defects in hair follicle, limb, neural, or testis development [17]. However, with age, homozygous mutant male mice developed skin lesions consisting of alopecia and epidermal hyperplasia, suggesting a role for *Ptch2* in adult epidermal homeostasis via Shh signaling. In accordance with the milder phenotype of *Ptch2*$^{-/-}$ than *Ptch1*$^{-/-}$, which is embryonic lethal [18], it is not surprising that individuals carrying a *PTCH2* mutation also exhibit milder clinical manifestations than those with classical NBCCS. Our patient lacked typical NBCCS phenotypes such as palmar/plantar pits, falx calcification, macrocephaly, hypertelorism and coarse face, the frequencies of which are 60.1, 79.6, 26.5, 68.8, and 27.9 %, respectively, in the Japanese population [9]. In fact, this case does not fulfill the criteria by Evans et al. [19] because a rib anomaly is considered to be a minor criterion. Since the number of cases with a *PTCH2* mutation is still limited, the accumulation of such patients is expected to further clarify their characteristic phenotype.

A genotype–phenotype correlation has not been reported in NBCCS patients [20]. However, mutations in the *SUFU* gene were reported to result in a much higher incidence of medulloblastoma than those in *PTCH1* [8, 14, 21]. It is also reported that a large genomic deletion encompassing *PTCH1* leads to NBCCS with atypical clinical manifestations, probably due to a deletion of adjacent gene(s) [12]. Therefore, it should be noted that NBCCS cases caused by a mutation of a gene other than *PTCH1* have phenotypes different from those of classical NBCCS caused by *PTCH1* mutations.

Acknowledgments This research was supported by Science Research Grants for intractable diseases in Japan (H22-intractable diseases-120) from the Ministry of Health, Labour and Welfare, and by a Grant-in-Aid for Scientific Research (20591261) from the Ministry of Education, Culture, Sports, Science and Technology.

Conflict of interest The authors declare that they have no conflict of interest.

References

1. Gorlin RJ (1987) Nevoid basal-cell carcinoma syndrome. Medicine (Baltimore) 66:98–113
2. Johnson RL, Rothman AL, Xie J, Goodrich LV, Bare JW, Bonifas JM, Quinn AG, Myers RM, Cox DR, Epstein EH Jr, Scott MP (1996) Human homolog of *patched*, a candidate gene for the basal cell nevus syndrome. Science 272:1668–1671
3. Hahn H, Wicking C, Zaphiropoulous PG, Gailani MR, Shanley S, Chidambaram A, Vorechovsky I, Holmberg E, Unden AB, Gillies S, Negus K, Smyth I, Pressman C, Leffell DJ, Gerrard B, Goldstein AM, Dean M, Toftgard R, Chenevix-Trench G, Wainwright B, Bale AE (1996) Mutations of the human homolog of Drosophila *patched* in the nevoid basal cell carcinoma syndrome. Cell 85:841–851
4. Ingham PW, McMahon AP (2001) Hedgehog signaling in animal development: paradigms and principles. Genes Dev 15:3059–3087
5. Smyth I, Narang MA, Evans T, Heimann C, Nakamura Y, Chenevix-Trench G, Pietsch T, Wicking C, Wainwright BJ (1999) Isolation and characterization of human *patched 2* (*PTCH2*), a putative tumour suppressor gene in basal cell carcinoma and medulloblastoma on chromosome 1p32. Hum Mol Genet 8:291–297
6. Fan Z, Li J, Du J, Zhang H, Shen Y, Wang CY, Wang S (2008) A missense mutation in PTCH2 underlies dominantly inherited NBCCS in a Chinese family. J Med Genet 45:303–308
7. Fujii K, Kohno Y, Sugita K, Nakamura M, Moroi Y, Urabe K, Furue M, Yamada M, Miyashita T (2003) Mutations in the human homologue of *Drosophila patched* in Japanese nevoid basal cell carcinoma syndrome patients. Hum Mutat 21:451–452
8. Kijima C, Miyashita T, Suzuki M, Oka H, Fujii K (2012) Two cases of nevoid basal cell carcinoma syndrome associated with meningioma caused by a *PTCH1* or *SUFU* germline mutation. Fam Cancer 11:565–570
9. Endo M, Fujii K, Sugita K, Saito K, Kohno Y, Miyashita T (2012) Nationwide survey of nevoid basal cell carcinoma syndrome in Japan revealing the low frequency of basal cell carcinoma. Am J Med Genet A 158A:351–357
10. Kimonis VE, Goldstein AM, Pastakia B, Yang ML, Kase R, DiGiovanna JJ, Bale AE, Bale SJ (1997) Clinical manifestations in 105 persons with nevoid basal cell carcinoma syndrome. Am J Med Genet 69:299–308
11. Nagao K, Fujii K, Saito K, Sugita K, Endo M, Motojima T, Hatsuse H, Miyashita T (2011) Entire PTCH1 deletion is a common event in point mutation-negative cases with nevoid basal cell carcinoma syndrome in Japan. Clin Genet 79:196–198
12. Fujii K, Ishikawa S, Uchikawa H, Komura D, Shapero MH, Shen F, Hung J, Arai H, Tanaka Y, Sasaki K, Kohno Y, Yamada M, Jones KW, Aburatani H, Miyashita T (2007) High-density oligonucleotide array with sub-kilobase resolution reveals breakpoint information of submicroscopic deletions in nevoid basal cell carcinoma syndrome. Hum Genet 122:459–466
13. Kosaki R, Nagao K, Kameyama K, Suzuki M, Fujii K, Miyashita T (2012) Heterozygous tandem duplication within the *PTCH1* gene results in nevoid basal cell carcinoma syndrome. Am J Med Genet A 158A:1724–1728
14. Taylor MD, Liu L, Raffel C, Hui CC, Mainprize TG, Zhang X, Agatep R, Chiappa S, Gao L, Lowrance A, Hao A, Goldstein AM, Stavrou T, Scherer SW, Dura WT, Wainwright B, Squire JA, Rutka JT, Hogg D (2002) Mutations in SUFU predispose to medulloblastoma. Nat Genet 31:306–310
15. Pastorino L, Ghiorzo P, Nasti S, Battistuzzi L, Cusano R, Marzocchi C, Garre ML, Clementi M, Scarra GB (2009) Identification of a SUFU germline mutation in a family with Gorlin syndrome. Am J Med Genet A 149A:1539–1543
16. Holbrook JA, Neu-Yilik G, Hentze MW, Kulozik AE (2004) Nonsense-mediated decay approaches the clinic. Nat Genet 36: 801–808
17. Nieuwenhuis E, Motoyama J, Barnfield PC, Yoshikawa Y, Zhang X, Mo R, Crackower MA, Hui CC (2006) Mice with a targeted mutation of patched2 are viable but develop alopecia and epidermal hyperplasia. Mol Cell Biol 26:6609–6622
18. Goodrich LV, Milenkovic L, Higgins KM, Scott MP (1997) Altered neural cell fates and medulloblastoma in mouse patched mutants. Science 277:1109–1113
19. Evans DG, Ladusans EJ, Rimmer S, Burnell LD, Thakker N, Farndon PA (1993) Complications of the naevoid basal cell carcinoma syndrome: results of a population based study. J Med Genet 30:460–464
20. Wicking C, Shanley S, Smyth I, Gillies S, Negus K, Graham S, Suthers G, Haites N, Edwards M, Wainwright B, Chenevix-Trench G (1997) Most germ-line mutations in the nevoid basal cell carcinoma syndrome lead to a premature termination of the PATCHED protein, and no genotype–phenotype correlations are evident. Am J Hum Genet 60:21–26
21. Brugieres L, Pierron G, Chompret A, Paillerets BB, Di Rocco F, Varlet P, Pierre-Kahn A, Caron O, Grill J, Delattre O (2010) Incomplete penetrance of the predisposition to medulloblastoma associated with germ-line SUFU mutations. J Med Genet 47:142–144

Congenital Anomalies
THE JAPANESE TERATOLOGY SOCIETY

doi:10.1111/j.1741-4520.2012.00362.x

Congenital Anomalies 2013; **53**, 49–53

CASE REPORT

Patient with terminal 9 Mb deletion of chromosome 9p: Refining the critical region for 9p monosomy syndrome with trigonocephaly

Norimasa Mitsui[1], Kenji Shimizu[2], Hiroshi Nishimoto[3], Hiroshi Mochizuki[4], Masao Iida[1], and Hirofumi Ohashi[2]
[1]Department of Clinical Laboratory, Divisions of [2]Medical Genetics, [3]Neurosurgery, and [4]Metabolism and Endocrinology, Saitama Children's Medical Center, Saitama, Japan

ABSTRACT **We describe a patient with typical manifestations of 9p monosomy syndrome, including trigonocephaly and sex reversal. Array comparative genomic hybridization (CGH) revealed a 9p terminal deletion of approximately 9 Mb with the breakpoint at 9p23. We compared the deleted segments of 9p associated with reported cases of 9p monosomy syndrome with trigonocephaly. We did not identify a region that was shared by all patients; however, when only pure terminal or interstitial deletions that did not involve material from any other chromosome were compared, we identified a segment from D9S912 to RP11-439I6 of approximately 1 Mb that was deleted in every patient. We propose that this 1-Mb segment might be the critical region for 9p monosomy syndrome with trigonocephaly.**

Key Words: 9p monosomy, craniosynostosis, critical region, sex reversal, trigonocephaly

INTRODUCTION

Monosomy 9p syndrome [MIM 158170] is a rare but well-known chromosomal deletion syndrome characterized by distinct craniofacial features (including trigonocephaly), various systemic anomalies, developmental retardation, and occasional sex reversal in XY patients (Huret et al. 1988). Since Alfi et al. (1973) first described a patient with the syndrome, more than 100 patients, most with terminal deletions with breakpoints around 9p21-p23 based on chromosome G-band analysis, have been reported. Recent advances in molecular/cytogenetic techniques allow attempts to map the loci responsible for cardinal features of the syndrome, especially trigonocephaly and sex reversal. While *DMRT* genes, which map to the most terminal 9p24.3 band, have been elucidated as the genes responsible for sex reversal (Raymond et al. 1998; Ogata et al. 2001; Barbaro et al. 2009), no gene has yet been identified as definitively responsible for trigonocephaly. Moreover, previous studies have been inconsistent with regard to identification of the 9p regions that are responsible for trigonocephaly (Wagstaff and Hemann 1995; Christ et al. 1999; Kawara et al. 2006; Faas et al. 2007; Hauge et al. 2008; Swinkels et al. 2008; Shimojima and Yamamoto 2009). Here, we describe a patient with a terminal 9p deletion of approximately 9 Mb who has the typical clinical manifestations of 9p monosomy syndrome, including trigonocephaly and sex reversal.

CLINICAL REPORT

The girl patient was born by cesarean section after 38-week gestation to a 30-year-old gravida 2, para 1 mother and a 31-year-old father, both Japanese, healthy, and unrelated. The patient's birth weight was 2864 g (–0.5 SD), length 49.5 cm (+0.2 SD), and occipitofrontal head circumference 35.5 cm (+1.5 SD). The patient had a healthy older sister. The patient was referred to us at the age of 11 months because of developmental delay and skull deformity. The notable craniofacial features were trigonocephaly, ptosis of the eyelids, epicanthus, upslanting palpebral fissures, flat nasal bridge, broad nasal root, long philtrum, thin upper lip, and low-set ears. A skull computed tomography scan with 3D reconstruction confirmed trigonocephaly with metopic suture synostosis (Fig. 1). Fronto-orbital advancement with cranial reshaping was performed when she was 1 year and 3 months old. She showed normal female external genitalia. When the patient was 2 years old, an abdominal ultrasonography revealed a uterus, but no ovary or testis was detected. A test of human chorionic gonadotropin load suggested the existence of testis, while luteinizing hormone-releasing hormone load test revealed primary hypogonadism. She weighed 14 kg (–1.7 SD) and was 100.2 cm tall (–1.9 SD) at 5 years of age. Her development was moderately delayed, and her IQ was estimated to be around 40 with the Tanaka–Binet Intelligence Scale at the age of 6 years.

G-banding analysis at a resolution of 550-bands on metaphase chromosomes obtained from phytohemagglutinin-stimulated lymphocyte cultures from the patient revealed a distal deletion of the short arm of chromosome 9 with a breakpoint at 9p23 and an XY sex chromosome constitution (sex reversal) (Fig. 2). Her parents were chromosomally normal. Fluorescence *in situ* hybridization (FISH) using whole-chromosome painting probes for chromosome 9 and a subtelomeric probe for the short arm of chromosome 9 (both from Vysis/Abbott Molecular Inc., Des Plaines, IL, USA) revealed that the abnormal chromosome 9 did not contain translocated material from another chromosome. To further define the extent of the deleted region in 9p, we performed an array comparative genomic hybridization (CGH) analysis using the Agilent Human Genome 244 K CGH kit (Agilent Technologies, Santa Clara, CA, USA). The result showed a hemizygous 9.17 Mb terminal deletion of chromosome 9p and no other apparent pathogenic copy number variation was identified in the whole genome (Fig. 3). Her karyotype was designated as 46,XY,del(9)(p23).arr 9p23 (194 193-9 169 072)x1 dn. FISH analyses with bacterial artificial chromosome (BAC) clones spanning the region from 9p23 to 9p24 refined the breakpoint between the clones RP11-1134E16 (D9S2000) and RP11-74 L16 (D9S912) (Table 1). BACs containing *DMRT1* and *DMRT2*, both candidate genes for sex reversal (9p24.3), were confirmed to be in the deleted segment of 9p in the patient.

Correspondence: Hirofumi Ohashi, MD, PhD, Division of Medical Genetics, Saitama Children's Medical Center, 2100 Magome, Iwatsuki-ku, Saitama-shi, Saitama 339-8551, Japan. Email: ohashi.hirofumi@pref.saitama.lg.jp

Received January 20, 2012; revised and accepted February 9, 2012.

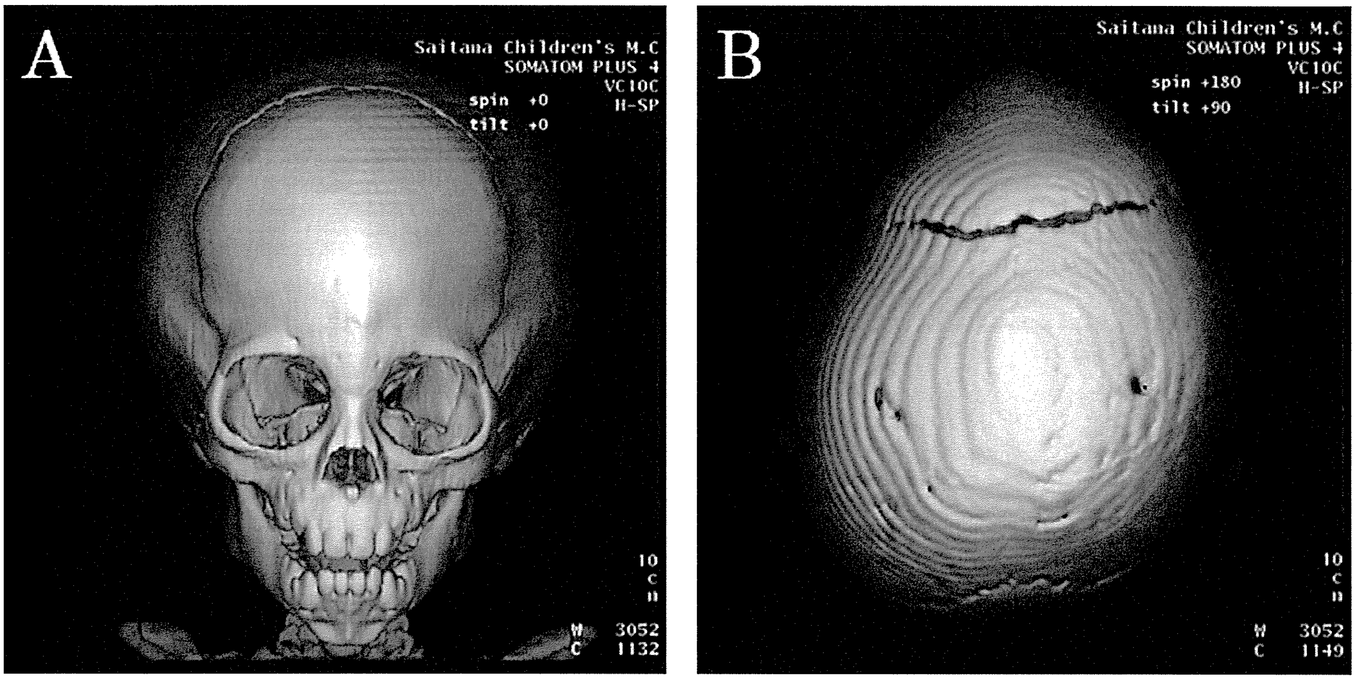

Fig. 1 Frontal (a) and top (b) views of the skull of the patient at age 11 months showing trigonocephaly, reconstructed by three-dimensional computed tomography.

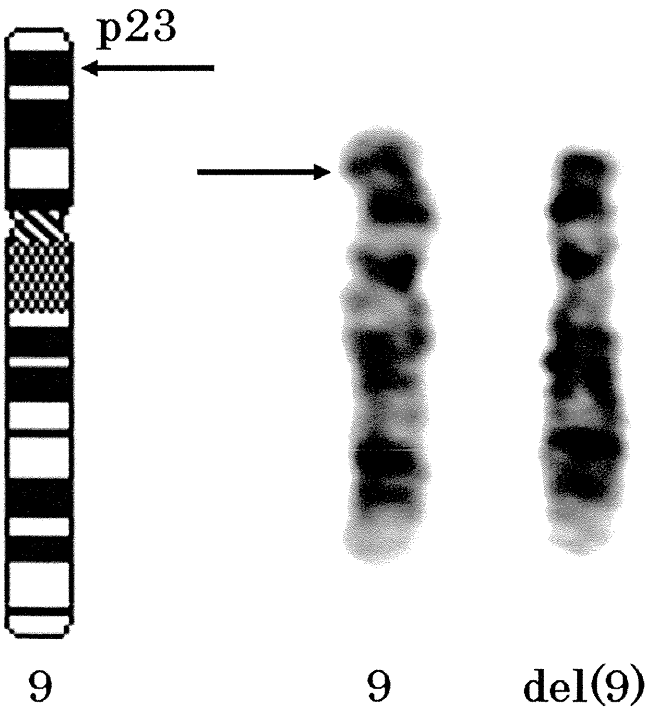

Fig. 2 G-banded partial karyotype of the patient showing a terminal deletion of chromosome 9. Arrow indicates the deletion breakpoint.

DISCUSSION

We described herein a girl patient with a terminal deletion of the short arm of chromosome 9 who had full manifestations of monosomy 9p syndrome, including distinctive craniofacial features (e.g. trigonocephaly, ptosis of the eyelids, epicanthus, upslanting palpebral fissures, flat nasal bridge, broad nasal root, low-set ears, long philtrum, thin upper lip), developmental delay, and XY sex reversal. Array CGH and FISH analyses revealed a pure terminal 9p deletion of approximately 9 Mb with the breakpoint between RP11-1134E16 and RP11-74 L16 at 9p23. *DMRT* genes, candidates for sex reversal (9p24.3), were included in the deletion in this patient.

Since Alfi et al. (1973) first reported 9p monosomy syndrome it has been established as a chromosomal deletion syndrome on the basis of G-banding cytogenetic analysis. Breakpoints in most patients with the syndrome, either with a pure terminal deletion or with a deletion associated with an unbalanced chromosome segment, reside around band 9p21-p23 (Huret et al. 1988). Recent advances in molecular techniques have allowed us to study precise correlations between the phenotype and karyotype/genotype associated with this syndrome. Wagstaff and Hemann (1995) first defined the critical region for 9p monosomy syndrome, including trigonocephaly, based on a boy with cryptic 9p monosomy, who was found to have a 9p deletion of approximately 11.6 Mb that included the region from D9S286 (9p24.1) to D9S162 (9p22.1); this deletion was associated with a translocation between 3p and 9p. Christ et al. (1999) studied 24 patients with 9p deletions (terminal deletions with or without unbalanced translocation), all of whom showed the consensus 9p-deletion phenotype (including trigonocephaly), and found that the minimum common deleted region is 16.1 Mb from D9S285 to the 9p terminal. Subsequently, several reports have been published that further define the critical region for the syndrome (Kawara et al. 2006; Faas et al. 2007; Hauge et al. 2008; Swinkels et al. 2008; Shimojima and Yamamoto 2009). Although, along with these works, some genes such as *CER1*, *TYRP1* and *PTPRD* have been postulated as possible candidate genes, no gene has yet been identified as conclusively responsible for the syndrome (Shimojima and Yamamoto 2009).

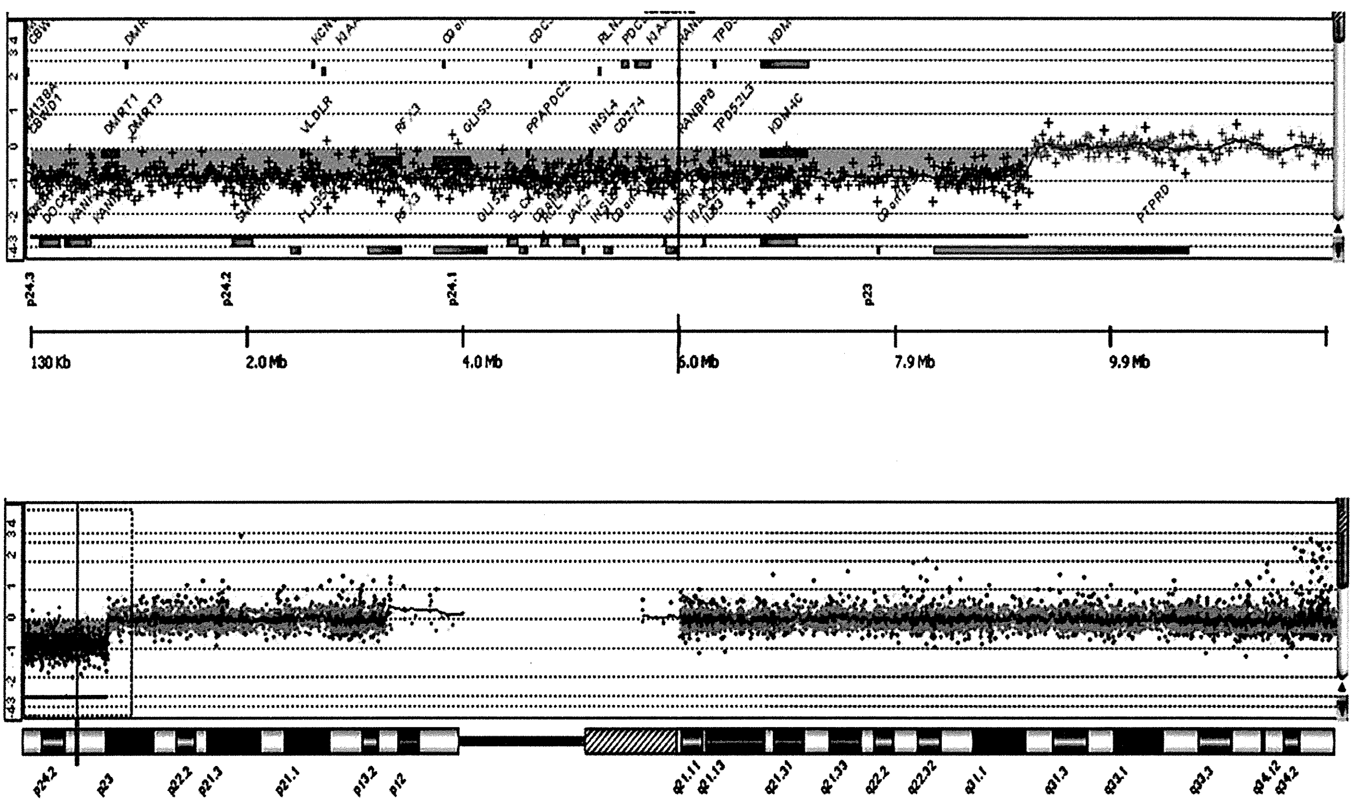

Fig. 3 Oligonucleotide array-CGH result of the patient. Whole chromosome view (lower) and close view (upper) of chromosome 9. Note a loss of 9.17 Mb of the terminal region of chromosome 9p.

Table 1 Fluoresence in situ hybridization (FISH) results using bacterial artificial chromosome clones and a subtelomeric probe around distal 9p

Probe name	Locus	Chromosome band	Distance from 9p terminal(Mb)	Signal on del(9p)
9p subtelomeric probe	–	9p24.3	–	–
RP11-143 M15	DMRT1	9p24.3	0.81	–
RP11-590E10	DMRT2	9p24.3	0.97	–
RP11-79 K3	–	9p24.1	7.30	–
RP11-29B9	D9S286	9p24.1	7.90	–
RP11-1134E16	D9S2000	9p23	8.99	–
RP11-74 L16	D9S912	9p23	9.26	+
RP11-176P17	D9S144	9p23	9.50	+
RP11-87N24	D9S168	9p23	10.47	+
RP11-58B8	–	9p23	11.60	+
RP11-382H24	D9S267	9p23	13.00	+

The distance from 9p terminal was retrieved from UCSC Genome Browser (NCBI 36/hg 18).

We compared deleted segments in all reported cases of 9p monosomy that were evaluated using molecular techniques (Fig. 4). Patients without trigonocephaly were not included in this comparison because penetrance of trigonocephaly might not be 100% and therefore considered unsuitable for use in phenotype mapping. While we could not find a common region that was shared by all patients, the segment from D9S912 to RP11-439I6, which is approximately 1 Mb, was deleted in the vast majority of the patients. There are only two patients who have a deletion that does not include this 1-Mb segment. The case reported by Kawara et al. (2006) had a more proximal interstitial deletion of 4.7 Mb at 9p22.3-p23. The chromosomal rearrangement in this patient was highly complex and

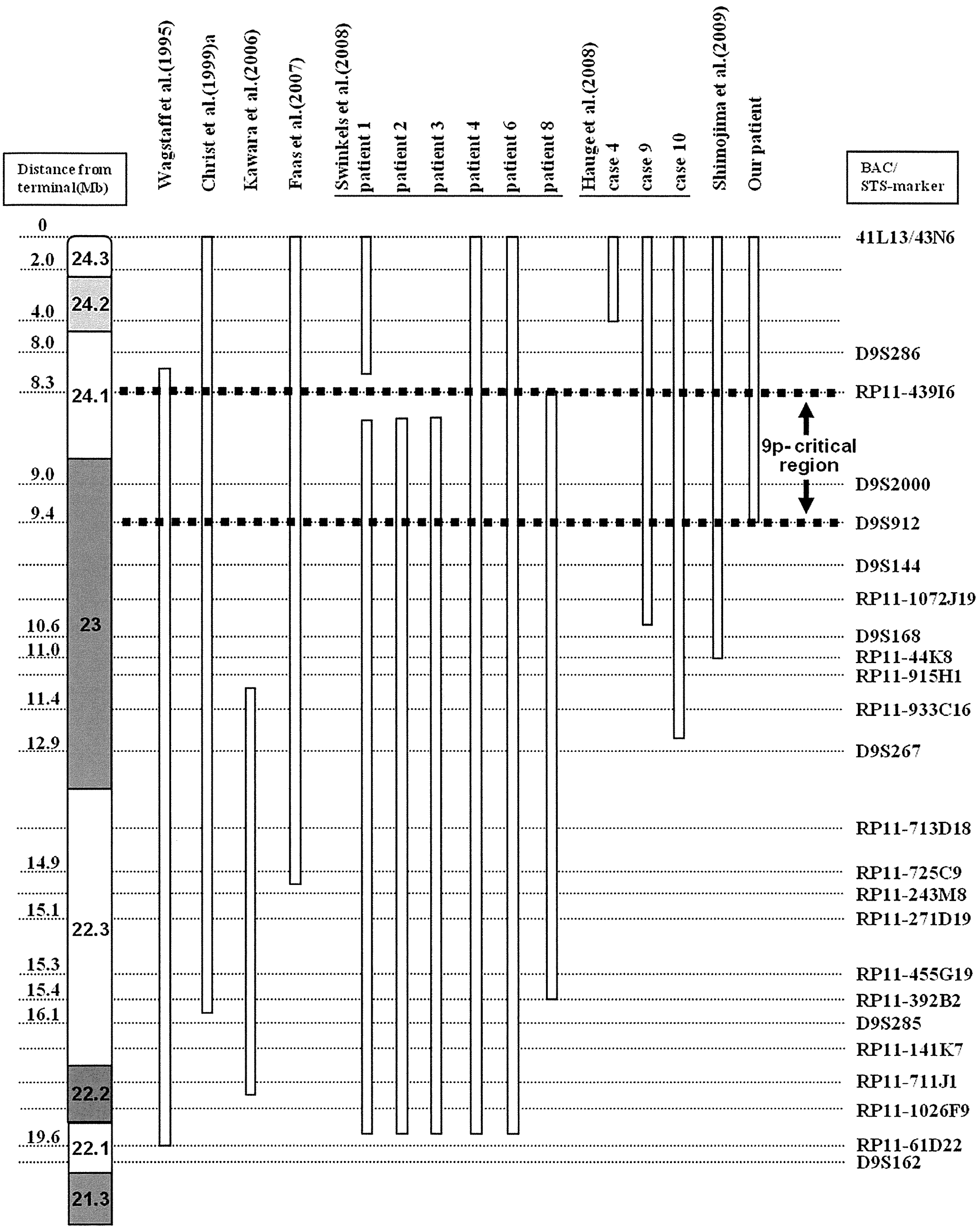
Distance from terminal(Mb)
Wagstaff et al.(1995)
Christ et al.(1999)a
Kawara et al.(2006)
Faas et al.(2007)
Swinkels et al.(2008)
patient 1
patient 2
patient 3
patient 4
patient 6
patient 8
Hauge et al.(2008)
case 4
case 9
case 10
Shimojima et al.(2009)
Our patient
BAC/ STS-marker
0
2.0
4.0
8.0
8.3
9.0
9.4
10.6
11.0
11.4
12.9
14.9
15.1
15.3
15.4
16.1
19.6
24.3
24.2
24.1
23
22.3
22.2
22.1
21.3
9p-critical region
41L13/43N6
D9S286
RP11-439I6
D9S2000
D9S912
D9S144
RP11-1072J19
D9S168
RP11-44K8
RP11-915H1
RP11-933C16
D9S267
RP11-713D18
RP11-725C9
RP11-243M8
RP11-271D19
RP11-455G19
RP11-392B2
D9S285
RP11-141K7
RP11-711J1
RP11-1026F9
RP11-61D22
D9S162

Fig. 4 Schematic map of the 9p deletion of reported cases of 9p monosomy, including the present case, evaluated using molecular analyses such as fluoresence in situ hybridization (FISH) and/or array comparative genomic hybridization. Open bars represent the presumed maximum extent of the deletion in each patient. a: the minimum common deleted region shared by 24 patients.

involved seven breakpoints on chromosomes 2 and 9. The patient, Case 4, reported by Hauge et al. (2008) showed a tiny terminal deletion of no more than 4 Mb. The karyotype of this patient was der(9)t(9;15) with a trisomic region from 15q(15q25-qter) that was translocated onto 9p24. That these two patients did not carry pure deletions of 9p may be noteworthy. Complex chromosome rearrangements are likely to have cryptic genome imbalance not only around the breakpoints but also at regions apart from the breakpoints. The altered chromosome constitution associated with unbalanced translocations might influence gene expression on the derivative chromosomes possibly through epigenetic modifications (Harewood et al. 2010). Obviously, it is preferable to choose pure terminal or interstitial deletion patients for genotype-phenotype mapping. In view of this preference and on the basis of comparison of deleted segments among patients with pure terminal or interstitial 9p deletion, including the present patient, we suggest the critical region for 9p monosomy syndrome, including trigonocephaly, might be a segment from D9S912 to RP11-439I6 of approximately 1 Mb. Of course, there are other possibilities: (i) the presence of multiple loci responsible for the syndrome and (ii) the presence of modifying factors that are located in different regions of the genome (Hauge et al. 2008). Further studies, such as using exome sequencing to screen cytogenetically normal patients with the 9p monosomy syndrome phenotype or with isolated trigonocephaly, might be necessary to identify the responsible gene for trigonocephaly of the 9p monosomy syndrome.

ACKNOWLEDGMENT

This study was funded in part by a grant from the Ministry of Health, Labour and Welfare, Japan, and from Kawano Masanori Memorial Foundation for Promotion of Pediatrics.

REFERENCES

Alfi O, Donnell GN, Crandall BF, Derencsenyi A, Menon R. 1973. Deletion of the short arm of chromosome no.9 (46,9p-): a new deletion syndrome. Ann Genet 16:17–22.

Barbaro M, Balsamo A, Anderlid BM et al. 2009. Characterization of deletions at 9p affecting the candidate regions for sex reversal and deletion 9p syndrome by MLPA. Eur J Hum Genet 17:1439–1447.

Christ LA, Crowe CA, Micale MA, Conroy JM, Schwartz S. 1999. Chromosome breakage hotspots and delineation of the critical region for the 9p-deletion syndrome. Am J Hum Genet 65:1387–1395.

Faas BH, de Leeuw N, Mieloo H, Bruinenberg J, de Vries BB. 2007. Further refinement of the candidate region for monosomy 9p syndrome. Am J Med Genet A 143A:2353–2356.

Harewood L, Schutz F, Boyle S et al. 2010. The effect of translocation-induced nuclear reorganization on gene expression. Genome Res 20:554–564.

Hauge X, Raca G, Cooper S et al. 2008. Detailed characterization of, and clinical correlations in, 10 patients with distal deletions of chromosome 9p. Genet Med 10:599–611.

Huret JL, Leonard C, Forestier B, Rethore MO, Lejeune J. 1988. Eleven new cases of del(9p) and features from 80 cases. J Med Genet 25:741–749.

Kawara H, Yamamoto T, Harada N et al. 2006. Narrowing candidate region for monosomy 9p syndrome to a 4.7-Mb segment at 9p22.2-p23. Am J Med Genet A 140:373–377.

Ogata T, Muroya K, Ohashi H, Mochizuki H, Hasegawa T, Kaji M. 2001. Female gonadal development in XX patients with distal 9p monosomy. Eur J Endocrinol 145:613–617.

Raymond CS, Shamu CE, Shen MM et al. 1998. Evidence for evolutionary conservation of sex-determining genes. Nature 391:691–695.

Shimojima K, Yamamoto T. 2009. Investigation of the candidate region for trigonocephaly in a patient with monosomy 9p syndrome using array-CGH. Am J Med Genet A 149A:1076–1080.

Swinkels ME, Simons A, Smeets DF et al. 2008. Clinical and cytogenetic characterization of 13 Dutch patients with deletion 9p syndrome: delineation of the critical region for a consensus phenotype. Am J Med Genet A 146A:1430–1438.

Wagstaff J, Hemann M. 1995. A familial 'balanced' 3;9 translocation with cryptic 8q insertion leading to deletion and duplication of 9p23 loci in siblings. Am J Hum Genet 56:302–309.

Focal Segmental Glomerulosclerosis in Patients With Complete Deletion of One *WT1* Allele

AUTHORS: Kazumoto Iijima, MD, PhD,[a] Tomonosuke Someya, MD, PhD,[b] Shuichi Ito, MD, PhD,[c] Kandai Nozu, MD, PhD,[a] Koichi Nakanishi, MD, PhD,[d] Kentaro Matsuoka, MD, PhD,[e] Hirofumi Ohashi, MD, PhD,[f] Michio Nagata, MD, PhD,[g] Koichi Kamei, MD, PhD,[c] and Satoshi Sasaki, MD, PhD[h]

[a]*Department of Pediatrics, Kobe University Graduate School of Medicine, Kobe, Japan;* [b]*Department of Pediatrics, Juntendo University School of Medicine, Tokyo, Japan;* [c]*Departments of Nephrology and Rheumatology, and* [e]*Pathology, National Center for Child Health and Development, Tokyo, Japan;* [d]*Department of Pediatrics, Wakayama Medical University, Wakayama, Japan;* [f]*Division of Medical Genetics, Saitama Children's Medical Center, Saitama, Japan;* [g]*Department of Pathology, Institute of Basic Medical Sciences, University of Tsukuba, Tsukuba, Japan; and* [h]*Department of Pediatrics, Hokkaido University Graduate School of Medicine, Sapporo, Japan*

KEY WORDS
deletion, focal segmental glomerulosclerosis, WAGR syndrome, *WT1*

ABBREVIATIONS

ACEI—angiotensin-converting enzyme inhibitor
BUN—blood urea nitrogen
CrCl—creatinine clearance
DDS—Denys-Drash syndrome
DMS—diffuse mesangial sclerosis
FSGS—focal segmental glomerulosclerosis
WAGR—Wilms' tumor, aniridia, genitourinary anomalies, and mental retardation

Each author contributed to the study as follows: Dr Iijima, patient management and manuscript writing; Dr Someya, patient management; Dr Ito, patient management; Dr Nozu, genetic analysis; Dr Nakanishi, genetic analysis; Dr Matsuoka, pathological analysis; Dr Ohashi, genetic analysis; Dr Nagata, pathological analysis; Dr Kamei, patient management; and Dr Sasaki, patient management.

www.pediatrics.org/cgi/doi/10.1542/peds.2011-1323

doi:10.1542/peds.2011-1323

Accepted for publication Jan 11, 2012

Address correspondence to Kazumoto Iijima, MD, PhD, Department of Pediatrics, Kobe University Graduate School of Medicine, 7-5-2 Kusunoki-Cho, Chuo-ku, Kobe 650–0017, Japan. E-mail: iijima@med.kobe-u.ac.jp

PEDIATRICS (ISSN Numbers: Print, 0031-4005; Online, 1098-4275).

Copyright © 2012 by the American Academy of Pediatrics

FINANCIAL DISCLOSURE: *The authors have indicated they have no financial relationships relevant to this article to disclose.*

FUNDING: This study was supported by Grants-in-Aid for Scientific Research (B) (to Dr Iijima, 20390240) from the Japan Society for the Promotion of Science.

abstract

The renal prognosis of patients with Wilms' tumor, aniridia, genitourinary anomalies, and mental retardation syndrome (WAGR) is poor. However, the renal histology and its mechanisms are not well understood. We performed renal biopsies in 3 patients with WAGR syndrome who had heavy proteinuria. The complete deletion of one *WT1* allele was detected in each patient by constitutional chromosomal deletion at 11p13 using G-banding, high-resolution G-banding, and fluorescence in situ hybridization. The patients exhibited proteinuria at the ages of 6, 10, and 6 years and were diagnosed as having focal segmental glomerulosclerosis (FSGS) at the ages of 7, 16 and 19 years, respectively. They exhibited normal or mildly declined renal function at the time of biopsy. Re-examination of a nephrectomized kidney from 1 patient revealed that some glomeruli showed segmental sclerosis, although he did not have proteinuria at the time of nephrectomy. The other 2 patients did not develop Wilms' tumor and thus did not undergo nephrectomy, chemotherapy, or radiotherapy, thereby eliminating any effect of these therapies on the renal histology. In conclusion, complete deletion of one *WT1* allele may induce the development of FSGS. Our findings suggest that haploinsufficiency of the *WT1* could be responsible for the development of FSGS. *Pediatrics* 2012;129:e1621–e1625

Downloaded from pediatrics.aappublications.org at N/A on May 18, 2012

Miller et al[1] first described WAGR syndrome (Wilms' tumor, aniridia, genitourinary anomalies, and mental retardation). Children with WAGR syndrome invariably have a constitutional chromosomal deletion at 11p13, the region where the *WT1* gene is located. Patients with Denys-Drash syndrome (DDS) usually have a germline missense mutation, which is predicted to result in an amino acid substitution in the eighth or ninth exon of *WT1*. Little et al[2] suggested that the severe nephropathy associated with DDS, which frequently leads to early renal failure, might result from the dominant-negative action of altered *WT1*. By contrast, because of the less severe genital anomalies and apparent lack of nephropathy associated with WAGR, a reduced *WT1* dosage during embryogenesis is thought to have a less pronounced effect on development, especially on renal system development.[3] Breslow et al[4] reviewed nearly 6000 patients enrolled in 4 clinical trials administered by the US National Wilms Tumor Study Group between 1969 and 1995. Of 22 patients with DDS, 13 (59%) developed renal failure; of 46 patients with WAGR, 10 (22%) developed renal failure. The cumulative risks of renal failure at 20 years were 62% and 38%, respectively. These findings suggest that nephropathy is not uniquely associated with missense mutations in *WT1* and that patients with the WAGR syndrome should be followed up closely throughout life for signs of nephropathy.

The renal prognosis of patients with WAGR is poor. However, the renal histology and its mechanisms are not well understood. We therefore performed renal biopsies to reveal the renal pathology in 3 patients with WAGR syndrome who had heavy proteinuria.

CASE REPORTS

Patient 1

Patient 1 was a male diagnosed with bilateral microphthalmos at 1 month of age. Wilms' tumor developed bilaterally at 3 years of age. He also had undescended testes and mental retardation. Previous analysis of G-banded metaphase chromosomes revealed a deletion of chromosome 11p13-15.1 in one allele[5]; the diagnosis of atypical WAGR syndrome was therefore made.[6] Because of a large tumor in the right kidney after the first chemotherapy treatment, the right kidney was nephrectomized. A diagnosis of nephroblastoma (nephroblastic type) was made. At the same time, the contralateral left kidney was biopsied, but no tumor was detected. The nephrectomized kidney revealed that there were no immature glomeruli, and a few glomeruli showed segmental sclerosis (Fig 1 A and B). The patient did not have proteinuria at the time of nephrectomy although microalbuminuria could have been detected.

The patient then underwent a second session of chemotherapy and radiotherapy treatment with left kidney protection. He developed heavy proteinuria at 6 years of age. The left kidney was biopsied (open biopsy) at age 7 years. Renal biopsy findings were consistent with focal segmental glomerulosclerosis (FSGS) (Fig 1 C and D). At the time of biopsy, the patient's height was 107.3 cm (−2.9 SD), weight was 21.7 kg (−0.7 SD), and blood pressure was 120/80 mm Hg. Biochemical data were as follows: total protein, 6.5 g/dL; albumin, 3.3 g/dL; blood urea nitrogen (BUN), 12.9 mg/dL; creatinine, 0.43 mg/dL; 24-hour creatinine clearance (CrCl), 72.2 mL/min/1.73 m^2; early morning urinary protein, 3+ (as measured by using a dipstick test); urinary protein to urinary creatinine ratio, 3.6 (milligram/milligram); and urinary β-2 microglobulin, 0.44 mg/dL (normal range: <0.23 mg/dL). His renal function gradually deteriorated despite angiotensin-converting enzyme inhibitor (ACEI) treatment. At 14 years of age, he underwent a preemptive living-related renal transplantation from his father.

Patient 2

Patient 2 was a male with aniridia, bilateral undescended testes, hypospadias, grade III to IV bilateral vesicoureteral reflux, and mental retardation. High-resolution G-banding revealed deletion of chromosome 11p13-p14.2 in one allele (Fig 2A), and fluorescence in situ hybridization showed heterozygous deletions of *PAX6*, *D11S2163*, *PER*, and *WT1* (Fig 2B), indicating WAGR syndrome. He had a single febrile urinary tract infection at 2 years of age and underwent an antireflux operation at 4 years of age, which resolved his vesicoureteral reflux. A dimercaptosuccinic acid radionuclide scan showed several defects in his right kidney. His proteinuria was detected at 10 years of age by the school urinary screening program. His proteinuria gradually increased, and he underwent renal biopsy (right kidney) at age 16 years. Renal biopsy findings were consistent with FSGS (Fig 1 E and F). At the time of biopsy, the patient's height was 169.2 cm, weight was 67.4 kg, and blood pressure was 128/78 mm Hg. Biochemical data were as follows: total protein, 6.8 g/dL; albumin, 4.3 g/dL; BUN, 25.0 mg/dL; creatinine, 1.20 mg/dL; 24-hour CrCl, 91.0 mL/min/1.73 m^2; early morning urinary protein, 3+ (as measured by using a dipstick test); urinary protein to urinary creatinine ratio, 2.7 (milligram/milligram); daily urinary protein, 3.1 g; and urinary β-2 microglobulin, 0.064 mg/dL. At the latest follow-up (24 years of age), his renal function was stable (BUN: 25.0 mg/dL; creatinine: 1.20 mg/dL) with ACEI treatment, and he had not developed Wilms' tumor.

Patient 3

Patient 3 was a female with aniridia and mental retardation. G-banding revealed deletion of chromosome 11p13-p14 in one allele (Fig 2C), and she was therefore diagnosed with WAGR syndrome. The patient developed proteinuria at

Downloaded from pediatrics.aappublications.org at N/A on May 18, 2012

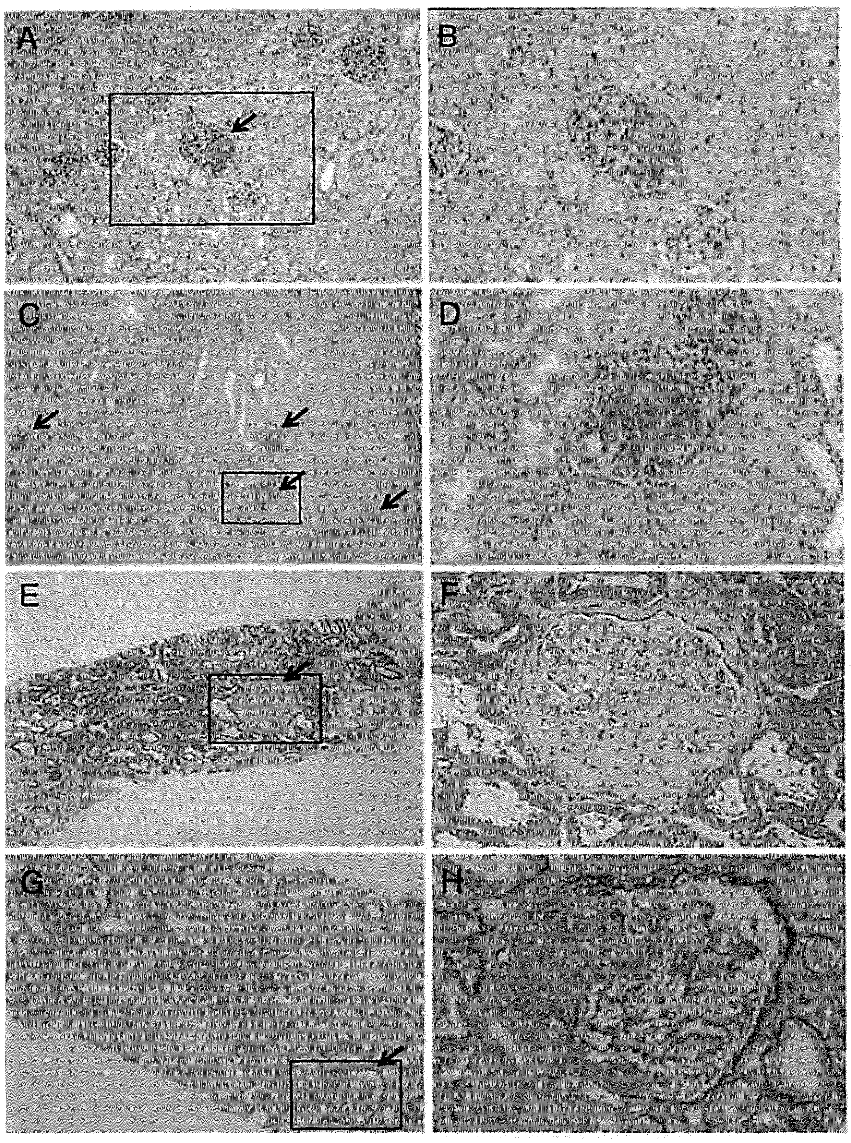

FIGURE 1
Renal histology. A, C, E, and G, Low magnification. B, D, F, and H, High magnification. Arrows show glomeruli with segmental glomerulosclerosis. A and B, Nephrectomized right kidney from patient 1. Patient 1 had no proteinuria at the time of nephrectomy. However, a few glomeruli exhibited segmental glomerulosclerosis although there were no immature glomeruli. C and D, Renal biopsy of left kidney from patient 1. Twenty-eight of 50 glomeruli showed segmental glomerulosclerosis. There were no tubulointerstitial lesions. E and F, Renal biopsy from patient 2. Two of eight glomeruli showed segmental glomerulosclerosis with interstitial fibrosis. G and H, Renal biopsy from patient 3. Ten of 30 glomeruli showed segmental glomerulosclerosis with interstitial fibrosis. All 3 patients exhibited FSGS (not otherwise specified).

the age of 6 years and nephrotic syndrome with normal renal function at age 15 years (urinary protein to urinary creatinine ratio, 10.6 [milligram/milligram]; total protein, 5.6 g/dL; albumin, 2.3 g/dL; BUN, 15.0 mg/dL; creatinine, 0.65 mg/dL; estimated glomerular filtration rate, 100.7 mL/min/1.73 m^2). We were unable to obtain her parents' consent for renal biopsy, and they chose to start drug treatment. However, treatment with prednisolone and ACEI was not effective, and her renal function gradually deteriorated. Therefore, she underwent renal biopsy at age 19 years. At the time of biopsy, her height was 144.5 cm, weight was 72.5 kg, and blood pressure was 130/83 mm Hg. Biochemical data were as follows: total protein, 5.5 g/dL; albumin, 2.5 g/dL; BUN, 30.0 mg/dL; creatinine, 1.40 mg/dL; 24-hour CrCl, 44.65 mL/min/1.73 m^2; early morning urinary protein, 3+ (as measured by using a dipstick test); daily urinary protein, 5.89 g; and urinary β-2 microglobulin, 0.495 mg/dL. Renal biopsy findings were consistent with FSGS (Fig 1 G and H). To date, she has not developed Wilms' tumor.

DISCUSSION

The current study demonstrated that 3 patients with atypical WAGR syndrome developed heavy proteinuria with FSGS, suggesting that the nephropathy seen in this syndrome is responsible for the FSGS lesion.

Patient 1 had possible bilateral Wilms' tumor and underwent unilateral nephrectomy, chemotherapy, and radiotherapy. Therefore, it is possible that the treatment of the remaining kidney for bilateral tumor or nephrogenic rest might account for the development of FSGS. However, the kidney nephrectomized after the first chemotherapy session but before radiotherapy treatment already showed segmental sclerosis in a few glomeruli, suggesting that radiotherapy was not the main cause of FSGS. Chemotherapeutic drugs such as adriamycin may induce FSGS as well as tubulointerstitial inflammation and fibrosis.[7] However, there were no tubulointerstitial lesions, suggesting that chemotherapy might not have been the main cause of FSGS. Nevertheless, it is possible that surgical renal ablation caused FSGS in patient 1.

Patients 2 and 3 did not develop Wilms' tumor during the course of clinical observation, and thus they did not undergo nephrectomy, chemotherapy, or radiotherapy, thereby eliminating any effect of these therapies on renal

Downloaded from pediatrics.aappublications.org at N/A on May 18, 2012